International Journal of Thermofluid Science and Technology (2021)
Volume 8, Issue 4, Paper No. 080403
https://doi.org/10.36963/IJTST.2021080403
Research Article

Experimental Investigation of a Thermal Plume's Air Entrainment in a Circular Cone

Ahmedou M. Mahmoud[1], Z.Yahya[2]

[1]*Unité de Recherche "Nouvelles Technologies de l'Energies et Systems Thermofluides nTEST",Département de Physique, Faculté des Sciences et Techniques, Université Alaasriya – Mauritanie*
[2]*Department of Physics, College of Science, Qassim University, P.O.Box 6644, Buraidah, 51452, Saudi Arabia*

ARTICLE INFO

Received: 28 May 2021;
Received in revised form:
21 Sept. 2021;
Accepted: 30 Sept. 2021;
Published online:
10 Oct. 2021

Keywords:
Air entrainment mode
Air entrainment coefficient
Thermal plume
Natural convection flow
Flow inside circular cone

ABSTRACT

In this study, we experimentally determined the effects of conical walls with low opening angles on a thermal plume's air entrainment. We first studied the development of a thermal plume placed at a specific height from the floor to ensure regular lateral and vertical air entrainment to a heat source. An analysis of the results showed the presence of two zones along the plume's height. The same plume source was then placed at the inlet of a vertical cone open at its extremities, which ensured purely vertical air entrainment. The convective transfer along the cone's walls as a function of the opening angles was studied to determine the critical angle ($\theta = 8°$) from at which the flow's thermal and dynamic characteristics began to improve. The resulting flow structure was divided into three distinct zones during its vertical development. The comparative study revealed that the cone walls radially widened the thermal plume and created a low recirculation region around the axis above the heat source. Due to the conical walls' effects, the relative increases in the plume width, mass flow rate, and convective heat flux in the plume were 20%, 25%, and 57%, respectively. The two configurations 'air entrainment coefficient increased by approximately 28% in the plume that developed inside the cone.

© Published at www.ijtf.org

1. Introduction

Studying air entrainment is essential to better understand the development of flow patterns encountered, for example, in fires, combustion chambers, and pollutant dispersion. This characterizes the plume's air transport; the air is drawn through the surface, limiting the plume. Stommel [1] first proposed the concept of air entrainment by studying the formation of a cumulus cloud using ambient air entrainment. Hougton and Cramer [2] further refined the study of air entrainment. They showed the difference between dynamic entrainment due to large-scale flow and turbulent entrainment caused by a turbulent mixture at the flow boundaries.

*Corresponding e-mail: ahmcheikho@gmail.com (Ahmedou M. Mahmoud)

The interaction between the plume and its environment affects the plume's dynamics and can be used to characterize the air entrainment. Several studies [3-8] indicated that the entrainment velocity of ambient air linearly varies with the plume flow's vertical velocity. This relationship's linearity constant is called the air entrainment coefficient, which is often treated differently by researchers [3, 4, 6-8]. This coefficient is an essential parameter of numerical or analytical plume flow modeling. Morton et al. [8] first proposed a one-dimensional model based on the self-similarity zone hypothesis to calculate the entrainment coefficient of a plume generated by a point source. Lee and Emmons [9] extended this model to plumes issuing from sources with finite dimensions. Morton's model's main limitation was its approximation of the presence of the entrainment coefficient's universal value. Therefore, the model cannot provide a convincing interpretation of the significant difference between the entrainment coefficient values of pure jets and pure plumes [10]. These studies were improved by List et al. [11] and Kotsovinos et al. [12]. In the absence of a reference physical theory of air entrainment, Tate [13] noticed a considerable variety in the entrainment coefficient values in these studies. Another calculation method was proposed to determine the air entrainment coefficient. Rico et al. [14] directly evaluated the entrainment coefficient using an original method that introduced a turbulent gas jet inside an air reservoir at uniform pressures. The air entrainment through a porous-walled cylindrical chamber was then measured to define the entrainment coefficient obtained using equation (15). Brahimi [15] used this equation to calculate a thermal plume's air entrainment coefficient induced by a heated disc and two identical interacting plumes (Table 2). Matulka et al. [16] experimentallystudied turbulent plumes developing in a calm non-stratified fluid medium under different source conditions. Other studies [3, 4, 11-14] indicated that air entrainment coefficientsvaried under different heat source conditions. Li et al. [17] performed experiments to determine the air entrainment characteristics of different heat source positions in a large space. The results indicated that the air entrainment coefficient was largely sensitive to different heat source positions with respect to the surrounding material environment.

The air entrainment mode of a thermal plume can also be elucidated by determining the flow development mechanisms and identifying the main zones during its vertical evolution. In this context, many researchers[15, 18-28] experimentally studied thermal plumes supplied by horizontal air entrainment that developed in an unlimited environment. Agator [18], and Brahimi and Son[19] studied turbulent thermal plumes issuing, respectively, from a hollow portion of a sphere and a circular disc heated at a constant and uniform temperature of 500 °C. These studies reported the appearance of two vertical zones. The first zone, just above the plume source, characterized the flow development region. This zone was followed by a second zone where the dynamic and thermal profiles were self-similar. This plume behavior was confirmed by Jaluria and Gebhart [20]. A similar experimental study on a turbulent plume generated by a disc heated uniformly at a temperature of 500 °C was conducted by Nakagome and Hirata[21], and George et al. [22]. They reported the presence of two zones that characterized the plume's vertical development; a first zone of buoyancy forces was followed by a second zone of self-similarity profiles. Other researchers [23, 24] reported the appearance of a small transition zone between two previously found zones. The transition region between laminar and turbulent thermal plume flows was determined by Yang [25]. The thermal and dynamic structures of two thermal plumes induced by a heated disc and heated vertical cylinder were studied by Bouzinaoui et al.[26]. They showed that the plume's flow structure in the two configurations was axisymmetric. To determine the source elevation's influence on a plume's air entrainment, Mahmoud et al. [27] experimentally studied a thermal plume induced by two heat sources placed at two different heights. The results showed that the air entrainment's vertical contribution changed the plume's structure.

Nomenclature

A	shape ratio $\left(A = \frac{2r_1}{H}\right)$	u	average air velocity, m.s^{-1}
C_p	specific heat, J.K-1.kg-1	u'	velocity fluctuating, m.s^{-1}
F_{ad}	flatness factor $\left(F_{ad} = \frac{\frac{1}{N}\sum_{i=1}^{N}(u_i - u)^4}{(\frac{1}{N}\sum_{i=1}^{N}(u_i - u)^2)^2}\right)$	u_i	instantaneous velocity, m.s^{-1}
F_{dd}	Skewness factor $\left(F_{dd} = \frac{\frac{1}{N}\sum_{i=1}^{N}(u_i - u)^3}{(\frac{1}{N}\sum_{i=1}^{N}(u_i - u)^2)^{\frac{3}{2}}}\right)$	U	dimensionless velocity $\left(U = \frac{u}{u_{ref}}\right)$
$F_{1\text{-}3}$	geometric configuration factor	u_{ref}	reference velocity $\left(u_{ref} = \frac{\nu H(Gr)^{\frac{1}{2}}}{r_0^2} = \sqrt{\frac{Hg(T_D - T_a)}{T_a}}\right)$, m.s^{-1}
Fr	Froude number $\left(F_r = \frac{u_{ref}}{\sqrt{gH}} = \sqrt{\frac{(T_D - T_a)}{T_a}}\right)$	u_{axe}	average air velocity measured at the plume axis (r = 0), m.s^{-1}
G	gravitational acceleration, m.s^{-2}	U_{axe}	dimensionless axial velocity $\left(U_{axe} = \frac{u_{axe}}{(u_{axe})_{max}}\right)$
Gr	Grashof number $\left(Gr = \frac{g\beta(T_D - T_a)r_0^4}{H\nu^2}\right)$	u_{max}	maximum average air velocity, m.s^{-1}
H	cone height, m	U_{max}	dimensionless maximum air velocity $\left(U_{max} = \frac{u_{max}}{u_{ref}}\right)$
I	electrical intensity, A	u_{min}	minimum average air velocity, m.s^{-1}
I_d	dynamic turbulent intensity $\left(I_d = \frac{\sqrt{u'^2}}{u}\right)$	V	electrical voltage, V
I_{daxe}	dynamic turbulent intensity at the plume axis (r = 0)	X	variable of the affinity $\left(X = \frac{r}{z - z_0}\right)$
K	air entrainment coefficient	z	vertical coordinate, m
M	momentum flow rate, kg.m.s^{-2}	Z	dimensionless height $\left(Z = \frac{z}{H}\right)$
Nu	Local Nusselt number	z_0	virtual origin where the plume appears to originate, m
Nu_m	mean Nusselt number		*Greek symbols*
P_r	heat flux radiated by the hot source, W	β	thermal expansion air coefficient, K^{-1} $\left(\beta = \frac{1}{T_a}\right)$
Pr	Prandtl number $\left(Pr = \frac{\nu}{\alpha}\right)$		
P_t	dimensionless convective heat flux	ν	kinematic fluid viscosity, m^2.s^{-1}
		α	Thermal diffusivity, m^2.s^{-1}
P_{v1}	heat flux provided from hot surface, W	λ	thermal conductivity, W.K^{-1}.m^{-1}
P_{v2}	heat flux from the hot wall, W	φ_{cv}	heat flux convective in the plume, W
q_m	mean mass flow rate, kg.m^{-3}	φ_e	electrical power, W
Q_m	dimensionless mean mass flow rate	φ_{em}	heat flux radiated by the ring, W
R	radial coordinate, m	φ_w	heat flux intercepted by the wall, W
r_0	radius of the hot disc, m	ρ	air density at mean temperature, kg.m^{-3}
r_1	large radius of the cone, m	ρ_0	air density at the reference temperature,kg.m^{-3}

r_2	radius of small section of the cone, m	ρ^*	dimensionless air density $\left(\rho = \frac{\rho}{\rho_0}\right)$
R	dimensionless radial coordinate $(R = r/r_1)$	σ	Stefann- Boltzmann constant, $W.m^{-2}.K^{-4}$
R^*	radius ratio $\left(R^* = r_0/r_1\right)$		*Subscripts*
$R_{0.5}$	half width of the plume	*a*	related to the air ambient
S	hot source surface, m^2	*axe*	related to the plume axis
S_c	cone radius ratio $\left(S_c = \frac{r_2}{r_1}\right)$	*D*	related to the hot disc
S_w	surface of the conical ring, m^2	*cv*	related to the total heat flux
T_1	average air temperature, K	*v1*	related to the heat flux from the source
T_a	ambient air temperature, K	*v2*	related to the heat flux from the wall
T_D	temperature of the hot disc, K	*r*	related to the thermal radiation
T_w	wall temperature, K	*ref*	related to the reference
T_0	dimensionless temperature $\left(T_0 = \frac{T_1 - T_a}{T_D - T_a}\right)$	*m*	related to the mean value
T_{max}	dimensionless maximum air temperature $\left(T_{max} = \frac{T_{1max} - T_a}{T_D - T_a}\right)$	*max*	related to the maximum value
T_∞	air temperature out boundary layer, K	*w*	related to the conical wall

The interactions between a thermal plume and vertical walls surrounding it generate complex mechanisms that could modify the air entrainment and the resulting flow structure. The flow structure resulting from these interactions was the subject of different investigations [28-34, 39]. The effects of a vertical wall placed near a plume's thermal source on the flow structure were studied by Agator and Son[28]. The results showed that the plume was pulled by the wall. Mahmoud [29] first studied the interaction of a thermal plume with a thermosiphon flow inside a heated vertical cylindrical wall. He showed that the plume was influenced by the walls' presence. Contrary to a free plume, the author reported the appearance of an additional zone in the plume's two classic zones. A first zone near the source was characterized by the formation of rotating rolls above the plume's heat source. The second zone was transitional, followed by a fully established turbulence zone. Building on these results, Zinoubi et al. [30] studied the form factors' effects on a plume flow structure. Using visualization and analyzing the flow structure, they confirmed the presence of three previously presented zones. Bouslimi [31] and Bouslimi and Dehmani[32] investigated vertical cylindrical walls' effects on a turbulent plume's lateral entrainment. They found that the plume's structure was divided into only two zones due to the source's lateral air entrainment. Naffouti et al. [33] studied the development of a thermal plume created by a rectangular heat source inside a vertical parallelepipedic canal open at the ends. They detected an important modification of the plume flow's turbulent structure. To simulate fires developing in tunnels, Saafi et al. [34] explored the turbulent structure of a thermal plume inside a rectangular tunnel with and without ventilation systems. They also showed the presence of three zones during the plume's vertical development.

An analysis of prior researches showed the absence of information on the interaction between a thermal plume, whose air entrainment is simultaneously lateral and vertical, and inclined walls despite the relative diversity of the walls used in these studies. Studying a thermal plume's development inside a cone is justified by its role in improving the understanding of the mechanisms involved in practical applications such as heat production in passive solar

systems, optimization of thermal comfort systems in solar homes, fires in buildings, and industrial chimney pollution. In addition to its importance from a fundamental perspective, using a cone allows heated air to be evacuated at the flow exit for possible future applications. Thus, it is interesting to clarify the vertical contribution's effects of air entrainment on a plume's dynamics when the source is symmetrically surrounded by inclined walls. In this study, the air entrainment's vertical contribution improved using a circular cone with small opening angles placed around the heat source.

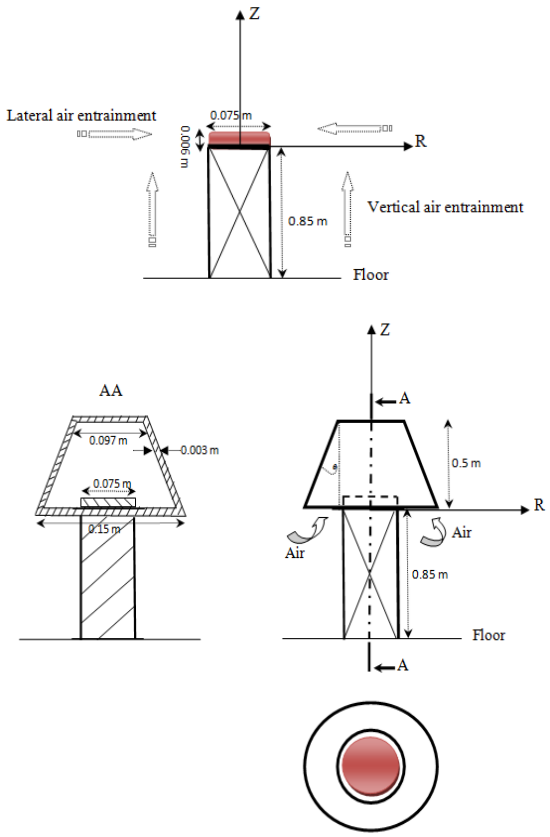


Fig.1. Studied System: (A). Free Thermal Plume – (B). Thermal Plume inside the cone.

This study explored the buoyancy flow development mechanisms and cone walls'effects on the vertical and lateral entrainment of a plume's air. We started by studying the flow structure of a free thermal plume fed by lateral and vertical air entrainment developed in an open medium (Fig.1A). The plume was then placed at a vertical cone's entrance open at the extremities with a low opening angle (Fig.1B). The cone's critical angle was determined before exploring the plume development mechanisms inside the cone. This work was completed by a comparative study of the plume's turbulent structure and air entrainment coefficient in the two investigated configurations.

2. Experimental Device and Measurement Tools

The experimental device and measurement techniques are shown in Fig.2. The numbers in this figure refer to the different parts of the experimental device and measurement tools used.

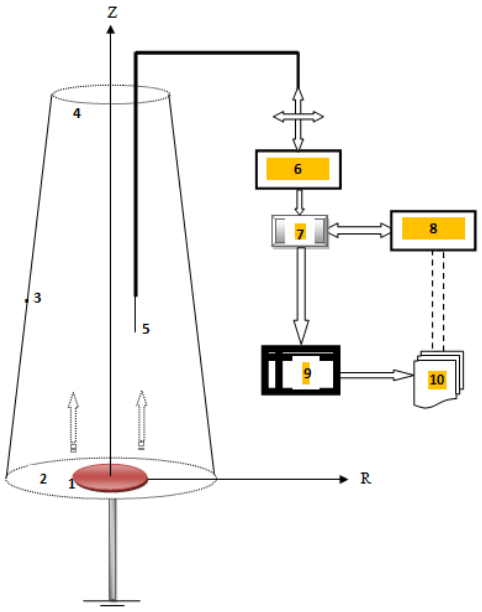
The experimental device was composed of a circular copper disc coated in matt blackand electrically heated at a uniform and constant temperature of 573 K. The disc was introduced at the vertical cone's inlet that was open at the extremities on a calm medium of a constant temperature (Fig.1). The cone was made of stainless steel coated in matt black. Cones with identical characteristics but small variable sections were also used. To decrease outside thermal losses, the cone walls were thermally insulated by a 0.02 m thick layer of Armflex. To facilitate vertical and lateral air entrainment, the disc was mounted 0.85 m above the floor. The plume's air temperature was precisely measured. The temperature distribution on the cone walls was measured at different heights using 9 Al-Cr thermocouples. The ratio between the cone's small and large radii was 0.65. The relative variation in the temperature along the heated disc's diameter was less than 2%.

The mean temperature and velocity fields were measured via hot wire anemometry. This measurement technique used the variations in the electric resistance of a platinum wire (with a 7.5 µm diameter and 3 mm length) with the air temperature [29-34, 36]. The wire's electrical resistance varied with the velocity and temperature of the plume's air [36]. Doan Kim-Son et al. [36] showed that an electrical intensity of 1.2 mA allowed a wire to be sensitive only to the air temperature, and an electrical intensity of 38 mA made it sensitive to the temperature and air velocity. The velocity and temperature of the plume's air

were determined by calibrating the voltage across the probe [36, 39]. To conduct the measurements without disturbing the flow, the wire remained constantly perpendicular to the ascending flow. The probe was placed vertically to the flow inside the cone. At low plume flow frequencies (not exceeding 3 Hz), the wire's thermal inertia (the wire's time constant was on the order of 1 ms) did not introduce any measurement errors into the air's temperature and velocity. In the range of studied velocities, the errors resulting from the probe calibration were contained in the interval $0.002 \leq \Delta U_e \leq 0.012$. At the air temperature calibration range, the errors were within the interval $0.003 \leq \Delta T_e \leq 0.01$. Standard errors on the used thermocouples vary between 0.0075 and 0.022.

To determine the plume's dynamic and thermal fields, a computer-controlled displacement system was used in two directions. The minimal displacement was 2 x10^{-5} m in the radial direction and 2 x 10^{-3} m along the height.

For statistical data processing, a device equipped with a digital card for data recording the acquired instantaneous signal values at 10 ms intervals and recorded the signals. The air plume's mean temperature and velocity values were determined by statistically treating the results. Due to the flow's sensitivity to environmental conditions, the experiments were conducted in a calm place. The experimental device was mounted inside a closed and large room (4m x 4m) so as to consider the plume environment as symmetrical and infinite. To control the ambient air temperature, six thermocouples were fixed at different positions from the experimental device. The average air temperature inside the room varies by a maximum of one degree (1°C) during a measurement day.



1. Hot disc; **2.** Cone's inlet; **3.** Al-Cr thermocouples; **4.** Cone's exit; **5.** Hot wire; **6.** Displacement system; **7.** Data logger; **8.** Data storage; **9.** Statistical data processing; **10.** Results storage.

Fig.2. Experimental Device and Measurement Techniques.

3. Determining the essential flow parameters

The heat source was placed at the inlet of a circular vertical cone open at the extremities (Fig.1B). The cone walls were heated by the effect of the heat flux radiated by the heat source, creating a thermosiphon flow around the plume.

3.1 Thermal balance

It was assumed that the surfaces of the cone walls and the heat source were black bodies (relatively high emissivities) and the air was a transparent medium.

At thermal equilibrium, the electrical power delivered by the plume source was:

$$\varphi_e = V.I (1)$$

Where V and I are the electrical voltage and intensity.

This power converted into thermal power was:

$$\varphi_e = P_{v1} + P_r (2)$$

P_{v1} and P_r represent the heat flux provided from the hot surface and the heat flux radiated by the hot source respectively.

The thermal flux provided by natural convection with the plume source was:

$$P_{v1} = \varphi_e - P_r \quad (3)$$

The thermal flux radiated by the plume source was:

$$P_r = \sigma S T_D^2 \quad (4)$$

Where S and T_D are the source's surface and temperature.

The cone walls were divided into circular rings coaxial at constant temperatures. Thermal balance was present in each ring. Fluxes radiated from other rings, and the cone's two extremities were negligible.

The thermal flux received by the cone walls was:

$$\varphi_w = F_{1_3} P_r \quad (5)$$

where F_{1_3} is the geometric configuration factor.

The heat flux radiated by the rings was:

$$\varphi_{em} = S_w \sigma T_w^4 \quad (6)$$

where S_w and T_w are the ring's surface and temperature.

The thermal flux radiated by the plume source heated the cone walls. The air absorbed the heat flux by natural convection with the heated walls. The thermal flux was:

$$P_{v2} = \varphi_w - \varphi_{em} \quad (7)$$

where P_{v2} is the heat flux from the hot wall.

The cone walls' local Nusselt number was:

$$N_u(z) = \frac{P_{v2} H}{(T_w - T_\infty)\lambda} \quad (8)$$

where λ is the air thermal conductivity, T_w and H are the cone's temperature and height. T_∞ is the air temperature outside the boundary layer.

The cone walls' mean Nusselt number was:

$$N_{um} = \frac{1}{H}\int_0^H N_u(z)dz \quad (9)$$

3.2 Determining the plume's convective thermal flux

The heat flux transferred by natural convection in a plume is an essential parameter for analytically determining the flow's thermal and dynamic characteristics.

The total heat flux resulting from heat exchange by natural convection with the heat source and cone walls was:

$$\varphi_{cv} = P_{v1} + P_{v2} \quad (10)$$

The total heat flux can be expressed as:

$$\varphi_{cv} = 2\pi C_p \int_0^{r(z)} \rho u r dr (T_1 - T_a) \quad (11)$$

where *r(z)* is the cone radius at the section *z*. T_i and u are the average air temperature and velocity. T_a the ambient temperature.

The dimensionless total convective heat flux inside the cone was:

$$P_t = \frac{\varphi_{cv}}{\pi \rho_0 C_p H \nu Gr^{\frac{1}{2}} (T_D - T_a)} = 2\int_0^1 URT_0 dR \quad (12)$$

where U is the dimensionless velocity, and R is the dimensionless radial coordinate. T_0 is the air dimensionless temperature.

3.3 Flow rate calculation

The mass flow rate(q_m) is an interesting thermal plume air entrainment parameter. It is determined by integrating the air velocity on a cone's radial section:

$$q_m = 2\pi \int_0^{r(z)} \rho r u dr \quad (13)$$

The dimensionless mass flow rate on a section of the cone was:

$$Q_m = \frac{2\pi \int_0^{r(z)} \rho r u dr}{\pi \rho_0 \nu H Gr^{1/2}} = 2\int_0^1 \rho^* U R dR \quad (14)$$

3.4 Air entrainment coefficient

The air entrainment coefficient K characterizes the transport of the fluid mass through the lateral surfaces of the plume.

According to an experiment conducted by Ricou et al. [14] on an isothermal jet, the air entrainment coefficient is expressed by:

$$K = \frac{1}{\sqrt{\rho_0 M}} \left(\frac{dq_m}{dz}\right) \quad (15)$$

where M is the momentum flow rate given by:

$$M = \int_0^\infty 2\pi \rho u^2 r dr \quad (16)$$

Equation (15) can be expressed as: $K = \frac{\frac{d}{dz}(2\pi \int_0^{r(z)} \rho u r dr)}{\sqrt{\rho_0 \int_0^{r(z)} 2\pi \rho u^2 r dr}}$ (17)

Prior studies [14, 15, 23] showed that this coefficient stabilizes in a plume's affinity zone. In this zone, it can be determined [15, 23] using the following relationship:

$$K = \frac{5}{3}\sqrt{2\pi} \frac{\int_0^1 \left(\frac{u}{u_{axe}}\right) X dX}{\sqrt{\int_0^1 \left(\frac{u}{u_{axe}}\right)^2 X dX}} \quad (18)$$

where X is a dimensionless variable used in the plume affinity theory. This variable makes it possible to plot self-similar profiles of the velocity and temperature, and to find the affine zone's similarity solutions of the plume flow. Here u_{axe} is the average air velocity measured at the plume axis ($r = 0$).

4. Results and discussions

Experimental work has been conducted for the following dimensionless numbers:
Grashof number Gr = 1.47 x 10^5
Prandtl number Pr = 0.75
Froude number Fr = 0.97

4.1. Thermal plume developing in an unlimited environment

4.1.1. Mean temperature and velocity fields of the flow

The axial distribution of the plume's dimensionless temperature and velocity means is shown in Fig.3. It was clear that these profiles developed in two different zones during the flow's vertical evolution. In the first zone closest to the heat source ($Z < 0.3$), the temperature and velocity gradients were relatively intense. The origin of these gradients' intensity was due to the flow acceleration induced by the dominant buoyancy forces. This zone was characterized by the flow's increased molecular viscosity due to the strong variations in the air's physical proprieties. At $Z = 0.3$, the maximum axial velocity was reached and the vertical gradient was zero. Thus, the buoyancy and viscous forces equilibrated. In the flow's superior part ($Z > 0.3$), the longitudinal gradients of the temperature and velocity decreased. In this zone, the flow deceleratedue to the dominant viscous forces.

This evolution was similar to that obtained in studies of plumes with lateral air entrainment [15, 18 – 24, 31]. Table 1 shows a quantitative comparison of extreme values of the free plume's averages temperature and velocity in previous works.The maximum values are measured at an altitude relatively close to the source (Z = 3 cm); while the minimum values are taken relatively far from the source. In fact, by comparison with a free plume with a lateral air entrainment, issuing from a disc heated at a temperature of 300 °C [31], one note relative differences of maximum averages velocity and temperature on the order of 32% and 27% respectively. These differences were due to the contribution of the vertical entrainment of the air. The shape of the plume source significantly affects the maximum temperature rather than the maximum velocity. It is clear that the semi-spherical shape of the plume source favors the air heating (relative increase of the air temperature of 38%) [15, 23]. In Figs.4 and 5, the radial distribution of the dimensionless temperature and velocity is presented in different sections, respectively.

In the section near the heat source ($Z < 0.3$), Fig.4 shows a relatively low temperature value located on the plume axis. The appearance of this minimum temperature was caused by the penetration of cool air under the effect of the air entrainment's vertical contribution.

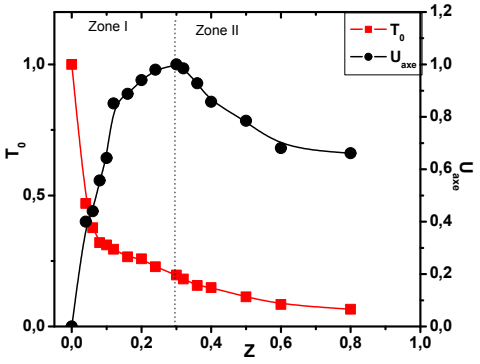


Fig.3. Axial development of the dimensionless average temperature and velocity of the free plume.

The temperature profiles showed the presence of strong transverse gradients on each side of the axis due to the air flow entrainment mechanisms. As the height increased, these gradients retained their intensity until they reached Z=0.3, where the profiles became flatter. This sudden reduction in the transverse thermal gradients reflected the appearance of a new regime in which the flow profiles became similar. Fig.5 indicates the presence of a strong transverse dynamic gradient on both sides of the axis. This significant velocity gradient was the main cause of the air entrainment on the plume's borders. The air entrained horizontally was added to the air entrained from below. This simultaneous entrainment of the air contributed to the plume flow's more active vertical transport. At Z = 0.3, Fig.5 shows that the global level of the vertical velocity decreased slightly in the central part and the profiles widened, indicating the presence of an established turbulent flow structure. Fig. 6 shows the vertical development of the plume

flow's maximal temperature and velocity. It was clear that the flow could be divided into two distinct zones.

4.1.2. Mass flow rate and convective heat flux in the plume

The convective thermal flux(P_t) and mass flow rate(Q_m) in a plume are essential parameters for numerically and analytically modeling the plume flow. We determined these parameters by numerically integrating equations (12) and (14).

Table 1
Comparison of main thermal and dynamic parameters of the free plume in previous works.

Author	Brahimi [15]	Guillou [23]	Boslimi [31]	Present work
Source (m)				
Plume	Disc ($2r_0$=0.07)	Hollow half sphere ($2r_0$=0.066)	++++++++++	Disc ($2r_0$=0.075)
Entrainment Mode	Air			
	Lateral	Lateral	Lateral	Lateral and vertical
T_D (°C)	50	500	300	300
T_{1max}(°C)	221	360	125	171
T_{1min}(°C)	40	42	36	38
u_{max}(m/s)	0.83	0.86	0.42	0.65
u_{min}(m/s)	0.32	0.28	0.10	0.10
I_{dmax}	0.34	0.45	--	0.2
I_{dmin}	0.15	0.12	--	0.05
F_{ad}	--	12	--	12
F_{dd}	--	2	--	12
Study	Exp.	Exp.	Exp. +Theo.	Exp. +Theo.

Fig.7 illustrates the vertical evolution of the plume's convective heat flux and mass flow rate. This figure's profiles indicate the growth of the mass flow rate with the plume height in the first zone, followed by the stabilization of its value in the zone with fully developed turbulence. This growth was attributed to the air entrainment at the plume's boundaries.

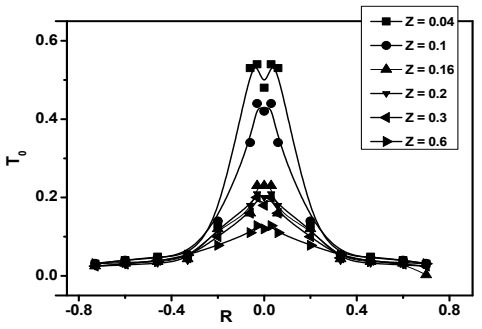


Fig.4. Radial development of the dimensionless average temperature of the free plume.

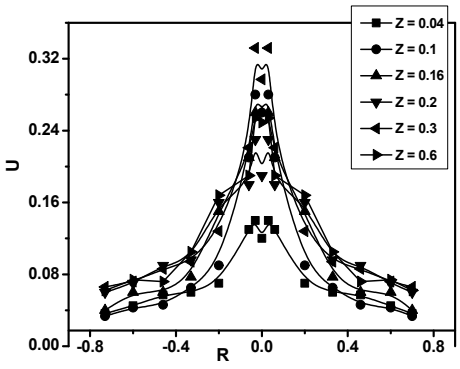


Fig.5. Radial development of the dimensionless average velocity of the free plume.

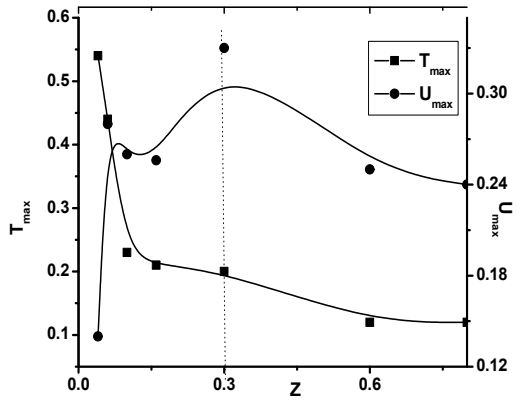


Fig.6. Vertical evolution of the maxima of the temperature and the velocity of the free plume.

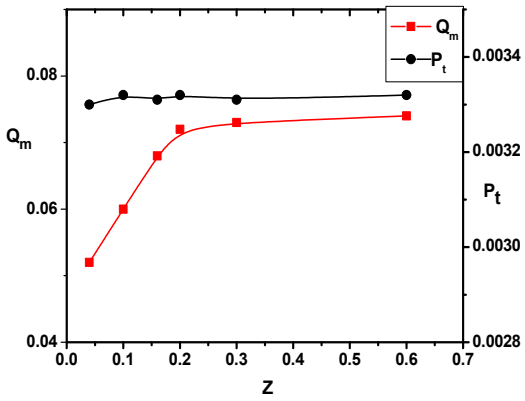


Fig.7. Vertical development of the dimensionless flow rate and the convective heat flux in the free plume

4.1.3. Air entrainment coefficient

Previous studies [13-17] show that the air entrainment coefficient remains constant within the affine zone of the plume. This zone starts from Z = 0.3 where the profiles are grouped around a single curve (Fig. 8). Thus, the air entrainment coefficient was determined by numerically integrating equation (18) using the experimental data in Fig. 8. This coefficient's value was K= 0.3. Compared with this coefficient's values in other studies (Table 2), this value was close to the value obtained by Ricouet al. [14]. This was attributed to the similarity of the air entrainment mechanisms in the two configurations, despite the difference of the flow generation conditions.

Table 2
Air entrainment coefficients

Authors	Nature of the plume	Entrainment coefficient (K)	Nature of the study
George et al. [22]	Hot jet	0.56	Theoretical
Nakagome et al. [21]	Thermal plume	0.67	Theoretical
Rico et al. [14]	Isothermal jet	0.28	Experimental
Brahimi [15]	Thermal plume	0.23	Experimental
Brahimi [15]	Plume in interaction	0.25	Experimental
List et al.[11]	Hot jet	0.43	Theoretical
Present work	Free plume	0.3	Experimental
Present work	Plume inside the cone	0.42	Experimental

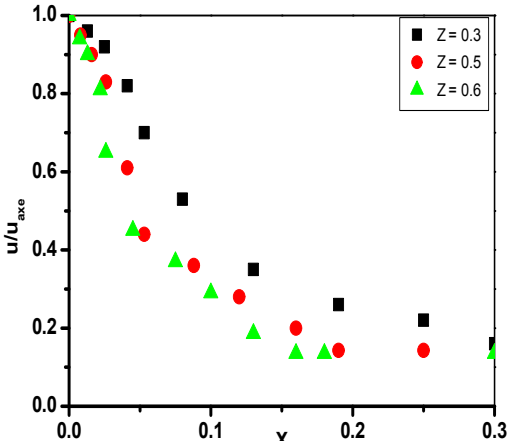


Fig.8. Radial distribution of the vertical velocity in the similarity zone of the free plume

4.1.4 Dynamic turbulent intensity

The axial distribution of the plume's dynamic turbulent intensity is presented in Fig.9. This evolution showed the separation of

the plume flow into two different zones. Fig.9 demonstrates the maximum turbulent intensity values at the level closest to the heat source. Thereafter, these values decreased from a minimal value at Z = 0.3 where the variations in the turbulent intensity completely changed form, indicating the start of a new flow regime. At Z= 0.3, the turbulent intensity increased and stabilized in the established turbulence zone. This evolution was qualitatively comparable to that described in several works [15, 18, 19, 23] studying a plume generated by a disc heated at 500 °C with lateral air entrainment. Nakagome and Hirata [21] were obtained a lower value of dynamic turbulent intensity (I_{dmax}=0.26) than that found by Brahimi [15], and a higher value than that found in the present work (Table 1). George et al. [22] measured a slightly higher intensity of turbulence (I_{dmax}= 0.28) for a plume issued from a hot air's jet. Table 1 shows that the maximum value of the dynamic turbulent intensity (I_{dmax} = 0.45) found by Guillou [23] is quite high compared to the values obtained by the other authors.This can be explained by the fact that the semi-spherical geometry of the plume source favors the turbulence increasing within the flow. Fig.10 shows the radial distribution of the plume's dynamic turbulent intensity in different sections. In the section near the heat source (Z=0.04), Fig.10 presents a structure with three maxima, one located on the plume axis and two located at the heat source's boundaries. As Z increased ($Z > 0.04$), the profiles showed a three-extrema structure with a minimal value located on the plume axis and two symmetrical maxima located close to the source borders. These maxima characterized the interactions between the plume and calm ambient fluid that surrounded it, causing air entrainment at the source's boundaries. The air entrainment was more important as the turbulence at the interface between the plume and the ambient air was elevated. The low turbulent intensity value indicated that the flow underwent acceleration under the buoyancy forces effect in the central region of the plume. The general view of these profiles differed from results obtained by Brahimi [15] in a thermal plume with air lateral entrainment. This difference was attributed to the vertical contribution of the air entrainment supplying the heat source from below[27].

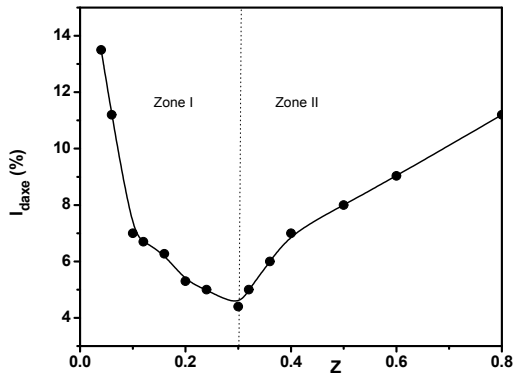


Fig.9. Axial development of the dynamic turbulent intensity of the free plume.

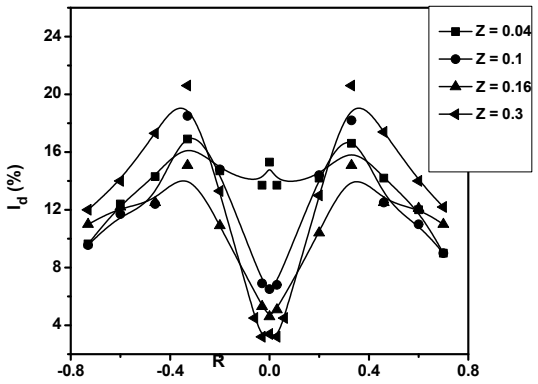


Fig.10. Radial development of the dynamic turbulent intensity of the free plume

4.1.5. Dynamic flatness and skewness factors of the plume

The radial distribution of the flow's flatness and skewness factors allowed a comparison between the probability density law of the velocity fluctuation distribution and the ideal Gaussian probability; these factors were F_{ad}=3 and F_{dd}= 0, respectively [29, 39].

Figs. 11 and 12 present the radial evolution of the flow's dynamic flatness and skewness factors, respectively, in different sections. In the sections close to the heat source ($Z < 0.16$), Fig.11 shows the presence of negative dynamic skewness values on the plume axis and at the edges of the heat source. These negative values indicated the presence of cool air eddies coming from the ambient environment caused by the plume entrainment. Fig. 12 shows the appearance of maximal dynamic flatness values located at the heat

source's boundaries. According to prior studies [29, 31, 38 and 39], these maximal values were attributed to the air intermittency at the plume's boundaries. Table 1 shows identical maximum values of F_{ad} located at the edges of plume sources of different geometry and temperature. These parameters generally give the same information about the plume flow regardless of the nature and temperature of the source.

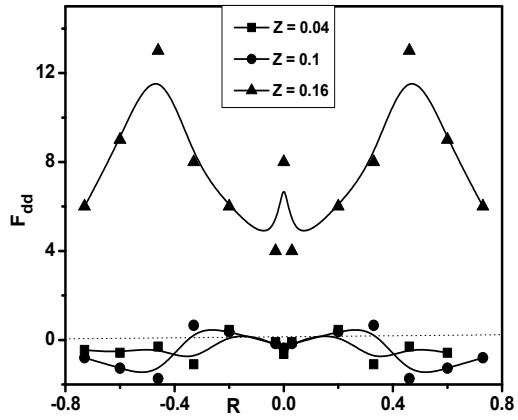


Fig.11. Radial distribution of the dynamic skewness factor of the free plume.

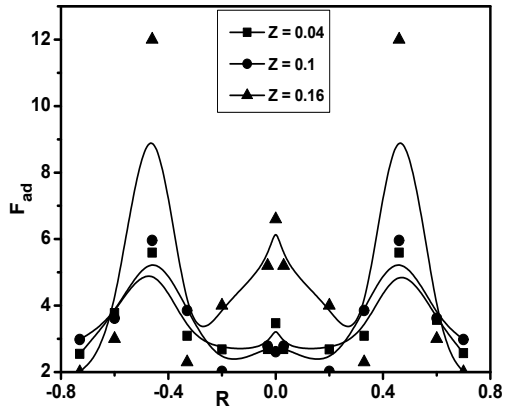


Fig.12. Radial distribution of the dynamic flatnesss factor of the free plume.

4.2. Thermal plume developing inside a vertical circular cone

4.2. 1. Determining the cone's critical angle

The Nusselt number was used to characterize the heat transfer by natural convection between the air and the conical wall. The local and mean Nusselt numbers were determined by numerically integrating equations (8) and (9) respectively.

The vertical development of the local Nusselt number on the cone walls at different opening angles is presented in Fig.13A. It was clear that the profiles followed the same natural convection transfer distribution between the walls and plume air. At all of the angles, the profiles indicated that the greatest convective transfer value with the walls was obtained at the cone's entrance and the least value was found at the walls' upper end. This situation resulted from the increase in the air temperature under the effect of the flow passage along the cone's heated walls. Subsequently, the difference in the air temperature between the walls and plume decreased as the cone's height increased, so the convective heat transfer decreased. The profiles showed that the heat convective transfer along the cone walls at angles less than $\theta = 5°$ was approximately identical to the cylindrical walls' heat convective transfer ($\theta = 0°$). At an angle $\theta = 8°$, the heat transfer between the cone walls and air started to improve with a relative variation of 28%. At angles $\theta > 8°$, the heat transfer by natural convection with the walls increased by 3% more than at$\theta = 8°$.Table 3 presents the cone's main characteristics at different opening angles. Fig.13B shows the variations in the walls'mean Nusselt number at different cone opening angles. These results indicated that the critical cone angle at which the convective heat transfer between the walls and air began to improve was $\theta = 8°$.

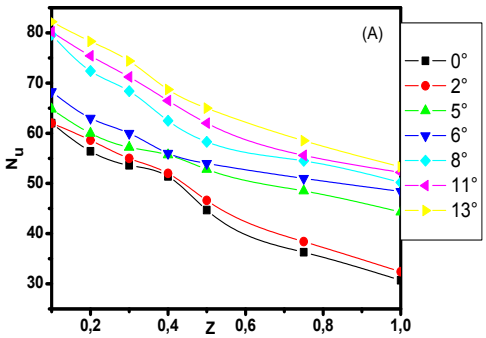


Fig.13-A. Vertical evolution of the local Nusselt number along the cone height for different opening angles.

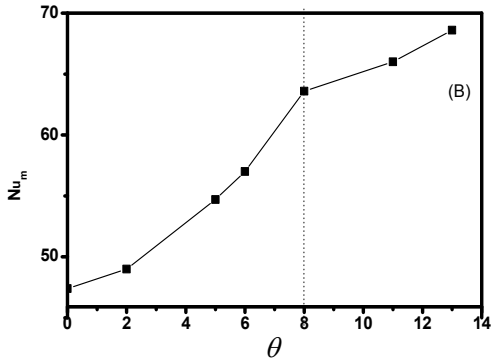


Fig.13-B. Evolution of the mean Nusselt number along the wall with opening angles of the cone.

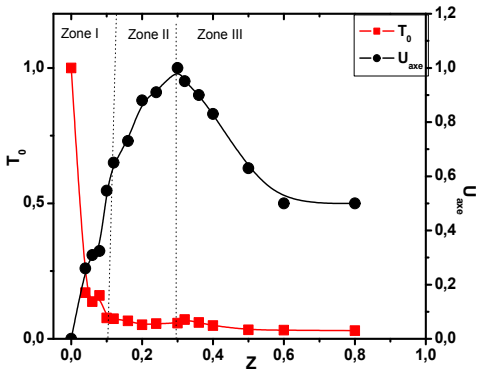


Fig.14. Axial development of the dimensionless average temperature and velocity of the plume inside the critical cone.

4.2.2. Study of the plume developing inside the critical cone

This experiment was conducted by fixing the following form factors:

- Ratio of the radii of the cone and the source R* = 0.5
- Shape ratio A = 0.3
- Cone radii ratio S_c = 0.65
- Critical cone angle $\theta = 8°$

4.2.2.1. The flow's mean temperature and velocity fields

Fig.14 illustrates the axial evolution of the dimensionless mean temperature and velocity of the thermal plume inside the critical cone. These profiles present three different variations in the air temperature and velocity along the plume axis. At $Z \leq 0.1$, the plume flow was strongly influenced by the heat source's location at the cone inlet. Along this zone, the variations in the air temperature and velocity were approximately low. This low variation was due to the presence of a small recirculation region centered on the source's axis where the air did not actively contribute to the flow development. In the second zone ($Z \leq 0.3$), the variations in the air temperature and velocity and the flow mixture began to activate. The maximum axial velocity was obtained when the balance of the viscosity and buoyancy forces occurred at Z = 0.3. In this section, a deceleration process began. The general evolution of these profiles was similar to those obtained in prior studies [29-33, 39].

Fig.15 shows the radial evolution of the plume flow's dimensionless mean temperature in different sections. In the zone near the heat source ($Z \leq 0.1$), the profiles had a three-extrema structure: two maxima located at R = 0.23 on either side of the plume axis and a minimum located on the axis. The temperature decrease on the axis was explained by the entrainment of cool air to feed the heat source at its axis. These profiles also highlighted the very strong transverse temperature gradient on the side of each maximum. This gradient was related to the strong variations in the air's physical properties with the temperature near the heat source. As Z increased, the maxima temperature decreased and approached the plume axis, but the gradients also remained important up to Z = 0.1, where the three-extrema profile disappeared, indicating the appearance of a new regime. In the intermediate sections ($Z \leq 0.3$), the profiles had only one maximum, and a sudden reduction in the transverse gradients was observed. In the last flow zone (Z = 0.6 and 0.8), the profiles became self-similar, indicating fully established turbulence.

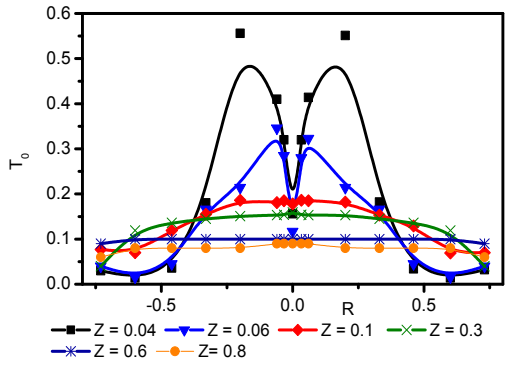


Fig.15. Radial distributions of the dimensionless air temperature of the plume inside the critical cone.

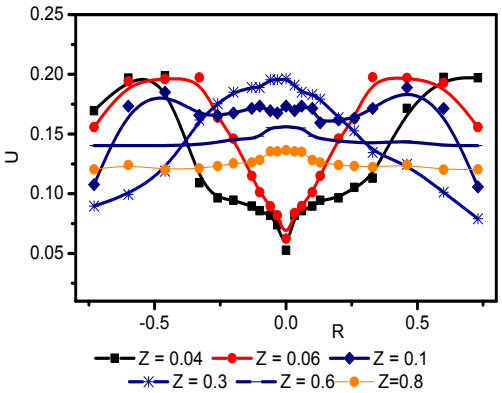


Fig.16. Radial distributions of the dimensionless air velocity of the plume inside the critical cone .

The radial evolution of the flow velocity's dimensionless mean vertical component in different sections is plotted in Fig.16. As shown by the axial distribution, the evolution of these profiles highlighted the presence of three different structures of the plume flow dynamics. In the sections close to the heat source ($Z \leq 0.1$), the profiles developed a three-extrema structure, with a low value located on the plume axis and two symmetrical maxima with respect to the axis. This three-extrema structure was found in other geometric configurations surrounding the plume [29, 31, 33, 39]. The minimum on the axis indicated the presence of a weak recirculation region in the central part above the heat source due to the dominant viscosity forces. In addition, the strong transverse gradients at the source's borders showed strong interactions with the ambient air, which characterized the lateral and vertical air entrainment. In the intermediate sections ($Z \leq 0.3$), Fig.16 shows the presence of a new structure in which the velocity profiles had a single maximum located on the axis. This new structure was characterized by a high vertical velocity near the axis and a relatively low velocity at the source's edges. This behavior indicated the presence of a strong ascending axial flow under the buoyancy force's influence. The rapid growth of the air velocity indicated the plume's contraction in this zone. Thus, to maintain constant thermal power, the plume flow's vertical velocity must increase as a result of the reduction in the plume section. The same development was reported by authors [27, 29, 38]. In the flow's upper part (Z=0.6 and 0.8), the profiles indicated a relative decrease in the plume velocity's global level. The shear forces were then relayed by the Reynolds stresses, which widened the plume. The profiles were self-reserving and grouped around a single curve (Fig.20), indicating the development of turbulence. In this zone, a relative increase in the flow velocity was observed near the plume axis. According to the flow continuity equation, the plume velocity increased through the cone's small section.

Fig.17 shows that the maxima gradually approached the plume's axis during the flow's vertical evolution. The profiles indicated that the evolution of the temperature maxima followed a linear variation and the maximum value appeared at the source's mid-radius(R=0.23), while the maximum velocity was found at the source's edges (R=0.45). Of note, the temperature variation's slope was greater than the velocity variation's slope. This behavior was attributed to the rotating rollers' development and escape [29, 31, 39]. The vertical development of the maxima of the temperature and velocity is illustrated in Fig.18. This evolution again showed the flow division's into three zones.

As reported in other studies [29, 31, 33, and 39], the appearance of the thermal and dynamic fields' three-extrema structure was attributed to the development and escape of the rotating rolls on the heat source. The cooler and denser air layers arriving from outside were located above the warmer and lighter layers adjacent to the heat source's surface.

This potentially unstable stratification caused the roller's formation.

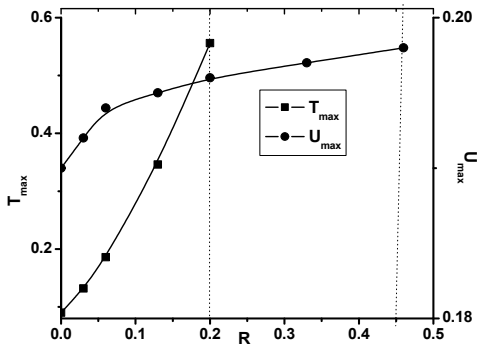


Fig.17. Radial evolution of the maxima of the plume's temperature and velocity inside the critical cone.

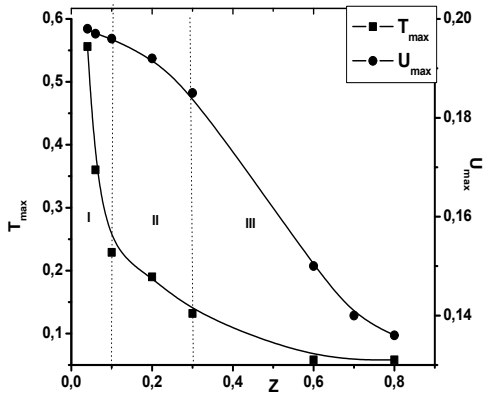


Fig.18. Vertical evolution of the maxima of the plume's temperature and velocity inside the critical cone.

4.2.2.2. Mass flow rate and convective thermal flux

The vertical development of the dimensionless convective thermal fluxand mass flow rateof the plume inside the cone is presented in Fig. 19. It was clear that these parameters developed constantly during the flow's vertical development. Table 3 shows that the cone walls intercepted most of the thermal flux radiated by the heat source (0.97%). Therefore, the air recovered the heat from the convective transfer with the heat source and cone walls and carried it to the flow exit. Thus, the thermal flux radiated by the heat source heated the plume air by recovering the heat from the cone walls. Thus, the thermal losses caused by the heat source's radiative flux were fully recuperated by natural convection with the heated walls.

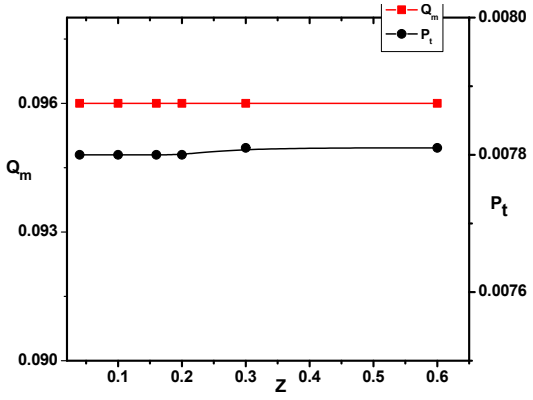


Fig.19. Vertical development of the dimensionless flow rate and the convective thermal flux of the plume inside the critical cone.

Table 3

Characteristics of the cone for different angles.

$\theta°$	F_{1-3}	P_t	Q_m
0	0.83	0.018	0.126
2	0.94	0.019	0.127
5	0.95	0.023	0.135
6	0.96	0.027	0.187
8	0.97	0.039	0.225
11	0.97	0.04	0.230
13	0.964	0.042	0.238

4.2.2.3. Air entrainment coefficient

The air entrainment coefficient was determined in the profile similarity zone by numerically integrating equation (18) using the experimental data in Fig. 20. The calculation results showed that the air entrainment coefficient was K= 42.

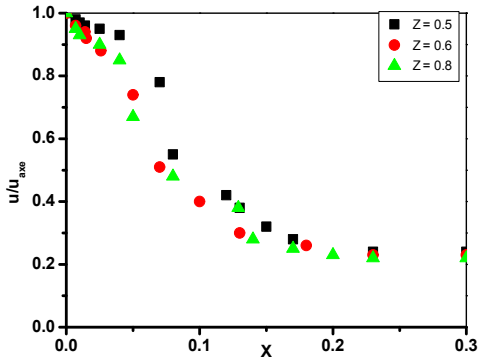


Fig.20. Radial distribution of the vertical velocity in the similarity zone of the thermal plume inside the critical cone.

4.2.2.4. Dynamic turbulent intensity

The axial distribution of the turbulence's dynamic intensity depending on the plume height is presented in Fig.21. This distribution clearly showed the appearance of three different zones in the flow's vertical development. In the first zone ($Z \leq 0.1$), the turbulence's dynamic intensity decreased from a maximal value near the source. It continued to decrease in the second zone ($0.1 < Z \leq 0.3$), reaching a minimal value at Z = 0.2. Then the dynamic intensity's behavior changed from Z = 0.3 by increasing and tended to stabilize in the flow's upper part ($Z > 0.3$). In the flow's central region corresponding to the second zone, it was clear that the turbulence's intensity was minimal, indicating that the flow accelerated due to the plume contraction's effects. Fig. 22 shows the turbulence intensity's radial distribution in different sections relatively close to the heat source. In the sections close to the plume source ($Z \leq 0.1$), the profiles shown the structure of a three-extrema variation, with a minimal value on the plume axis and two maxima symmetrical with respect to the axis. The two peaks corresponded to the plume region where the interaction between the flow and ambient air were maximal, making the air entrainment simultaneously radial and vertical due to the plume source. Beyond Z = 0.1, the three-extrema structure gradually widened and began to disappear at Z = 0.3, indicating the start of a new flow regime.

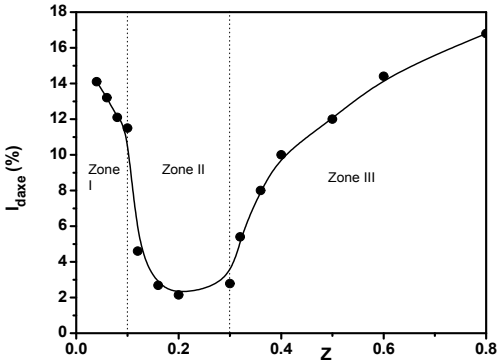


Fig.21. Axial development of the dynamic turbulent intensity of the plume inside the critical cone.

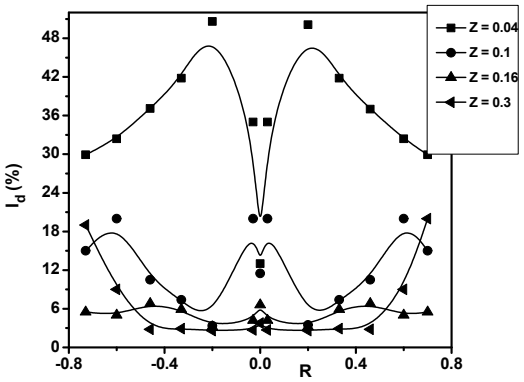


Fig.22. Radial development of the dynamic turbulent intensity of the plume inside the critical cone.

4.2.2.5. Dynamic flatness and skewness factors

The radial distributions of the flow's dynamic skewness and flatness factors are shown in Figs.23 and 24, respectively. In the sections closest to the source, Fig.23 shows the presence of a region around the plume axis in which the dynamic skewness factor was negative. These negative values confirmed a border separating the low velocity region located on the axis from the rest of the flow, where the probability law governing the fluctuations approached Gauss' ideal law. These negative values also indicated the presence of negative fluctuations at high amplitudes in this flow region. Of note, the negative skewness factors corresponded to the flow regions where the turbulence intensity was maximal [23, 27, and 29]. Fig.24 shows the dynamic flatness factor's two peaks at the heat source's boundaries. These maximum values characterize the presence of positive fluctuations induced by large structures interacting with the ambient air at borders of the hot source, under the effect of the air entrainment by the plume. The maximal dynamic flatness factor values on the source's axis corresponded to the minimum turbulence intensity values resulting from the flow's laminar nature in the zone close to the source.

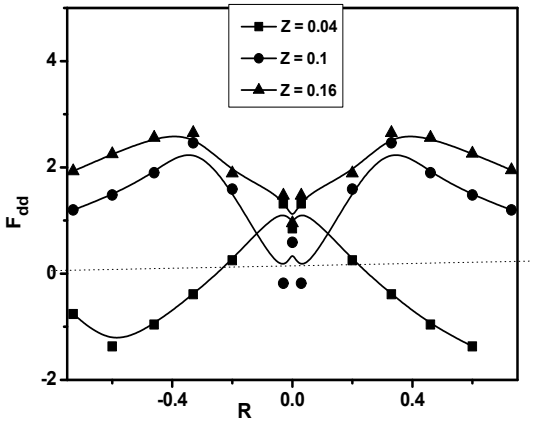


Fig.23. Radial distribution of the dynamic skewness factor of the plume inside the critical cone.

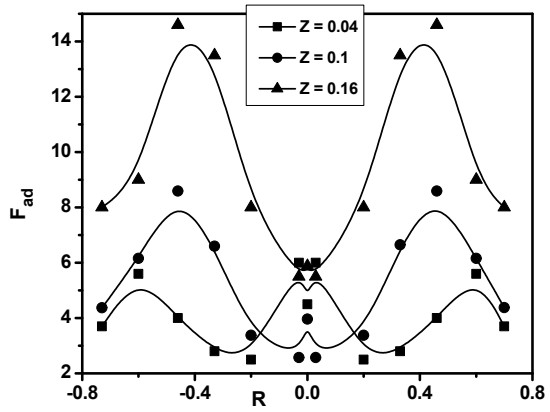
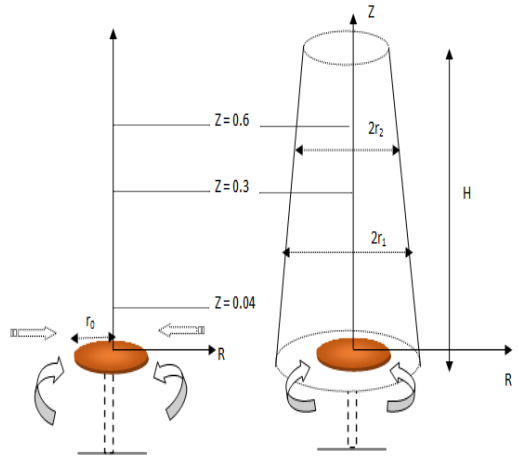


Fig.24. Radial distribution of the dynamic flatnesss factor of the plume inside the critical cone.

4.3. Comparative study

A comparative study was carried out between the flow sections as shown in Fig.25.



Configuration (A) **Configuration (B)**

Fig.25. Comparative StudyConfiguration (A): Free plume – Configuration (B): Plume inside the cone

4.3.1. The flow's mean temperature and velocity fields

Fig. 26 shows a comparison of the axial evolution of the plume's dimensionless mean temperature in the two situations studied. A comparison of the axial evolution of the flow velocity of the free plume and plume developing inside the cone is illustrated in Fig.27. These profiles show that the plume confinement's effects led to a relative decrease in the axial values of the flow's temperature and velocity. This decrease was attributed to the effects induced by the rotating rolls, which divided the flow in the zone close to the source into two symmetrical parts with respect to the plume axis. These two parts were separated by a low recirculation region centered on the source axis in which the temperatures and velocities were low. Thus, the cone walls caused an extenuation of the plume's axial development. In the zone relatively far from the heat source ($Z > 0.4$), the figure shows that the axial temperatures were closer in the two studied configurations, while the difference between the axial velocities remained high and fixed at a constant value. Figs.28(A-C) presents a comparison of the radial distribution of the plume's dimensionless mean temperature in the two studied configurations in three sections (Z = 0.04, 0.3, and 0.6). In the section closest to the heat source (Z = 0.04), Fig.28A indicates a radial widening of the plume's mean thermal field under the cone walls' effects. Thus, the two temperature maxima moved away from the plume axis and were located mid-radius from the source (R = 0.23). The temperature on the axis greatly decreased under the cone walls' effects. As observed by Agator [28], the cone's walls attracted the plume from the source's sides by creating a low temperature region around the axis. In the cone's central section (Z = 0.3), Fig.28B shows the flow's temperature uniformization under the effect of the plume's confinement inside the cone. The uniformization of the flow's temperature was clearly demonstrated in the cone's upper part (Fig. 28C). According to prior studies [29, 37, 39], this uniformization resulted from the development and escape of the rotating rolls on the heat source at the flow's entrance.

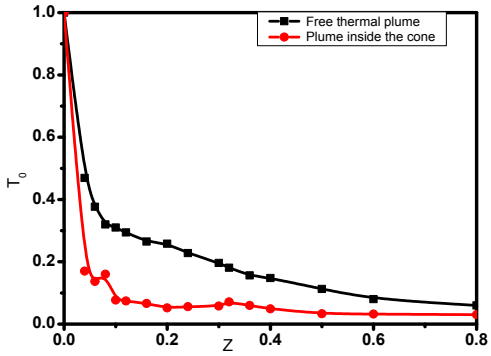


Fig.26. Comparison of the axial development of the dimensionless average temperature of the plume and the plume inside the cone.

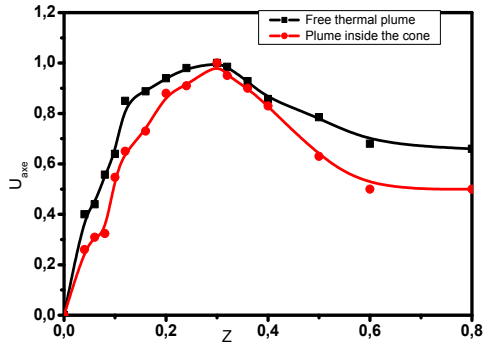


Fig.27. Comparison of the axial development of the dimensionless average velocityof the free plume and the plume inside the cone.

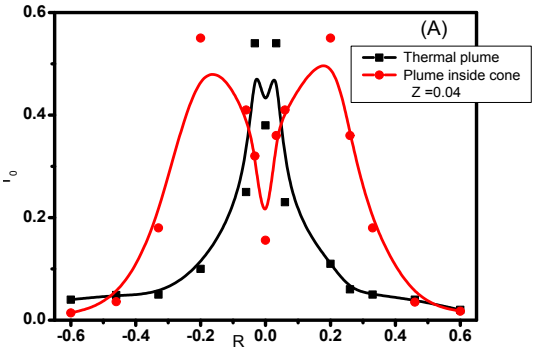


Fig.28. A. Comparison of the thermal profiles at the level closest to the source of the free plume and the plume inside the cone.

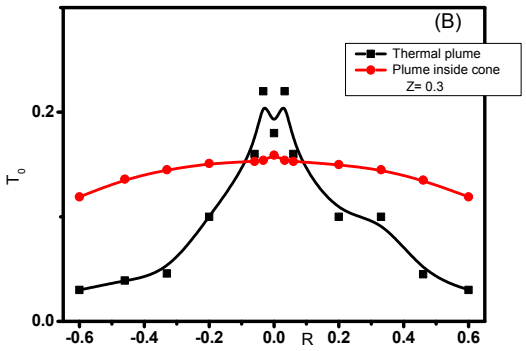


Fig.28. B. Comparison of the thermal profiles at the intermediate level of the free plume and the plume inside the cone .

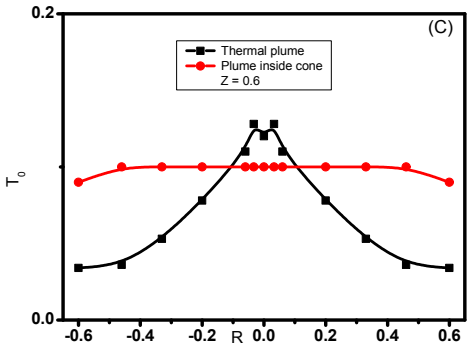


Fig.28. C. Comparison of the thermal profiles at the level far from the source of the free plume and the plume inside the cone.

Figs. 29(A-C) shows a comparison of the radial distribution of the plume's dimensionless mean velocity in the two configurations in three sections (Z = 0.04, 0.3, and 0.6). Fig. 29A shows the cone walls' significant effect on the plume development's dynamics in the section near the heat source (Z = 0.04). Thus, the plume was strongly attracted on either side of the axis by the cone's walls that surrounded it. The velocity maxima moved away from the axis and were located at the level of the source's edges. This widening of the dynamic field caused the appearance of a low recirculation axial region, larger than that observed in the thermal field. This behavior indicated that air entrainment occurred at the source's borders. In the cone's central section (Z = 0.3), Fig.29B indicates that the velocity weakened near the plume axis and slightly increased at the source's borders under the cone walls' effects. In this zone, the

confined plume's air velocity had a Gaussian shape, indicating that air entrainment occurred in the central part surrounding the axis and was limited by the source's edges. The uniformity of the flow velocity appeared in the cone's upper part (Fig. 29C) as consequence of the active mixing of air layers caused by the intensification of the vertical air entrainment leading to the development of the rotating rolls on the heat source's surface.

Fig. 30 shows a comparison of the plume width's vertical evolution in the two configurations. This figure demonstrates the significant increase in the lateral widening of the plume developing inside the cone, particularly from the flow's second zone (Z=0.3), where its relative growth was on the order of 20%. Thus, the cone walls caused a marked expansion of the thermal plume.

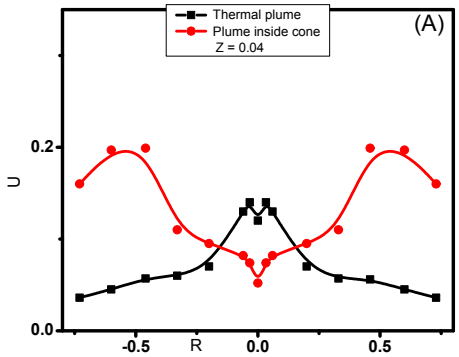


Fig.29. A. Comparison of the dynamic profiles at the level closest to the source of the free plume and the plume inside the cone.

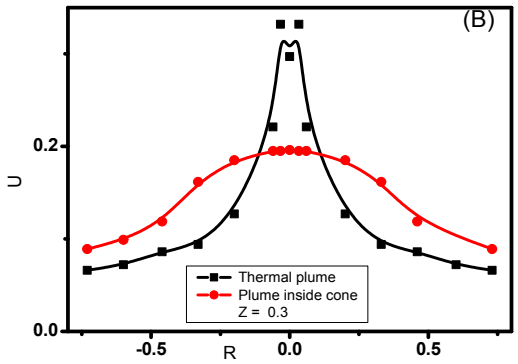


Fig.29. B. Comparison of the dynamic profiles at the intermediate of the free plume and the plume inside the cone .

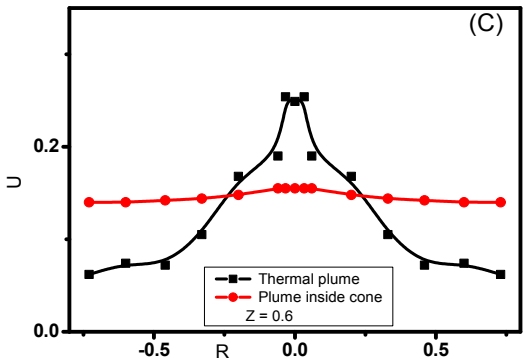


Fig.29. C. Comparison of the dynamic profiles at the level far from the source of the free plume and the plume inside the cone .

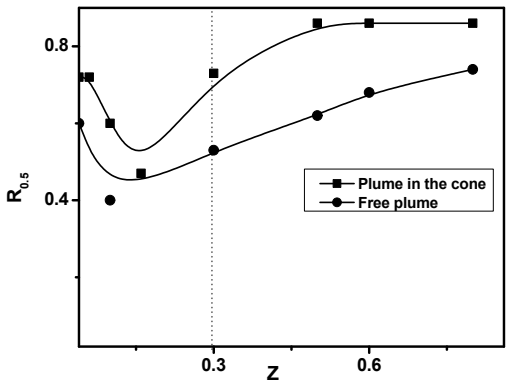


Fig.30. Comparison of the plume width.

4.3.2. Mass flow rate and convective thermal flux

Fig.31 presents a comparison of the mass flow rate development of the plume in the two configurations. This figure indicates the significant improvement in the mass flow rate under the cone walls' effects. In the free plume, the flow rate increased with the height until Z = 0.2, when it began to stabilize. This increase was due to the plume's lateral and vertical air entrainment. However, the flow rate of the plume developing in the cone was practically constant, indicating air entrainment only from the plume's bottom. The relative increase in the mass flow rate under the cone walls' effects was 25%. A comparison of the vertical development of the plume's convective thermal flux in the two configurations is plotted in Fig. 32.This figure profiles show the two configurations' practically constant heat fluxes. Near the cone's heated walls, the heat flux transferred by natural convection in the confined plume

improved, with a relative increase of 57%.

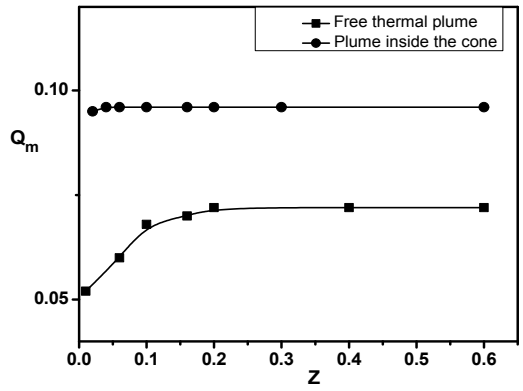


Fig.31. Comparison of the development of the plume flow rate of the free plume and the plume inside the critical cone.

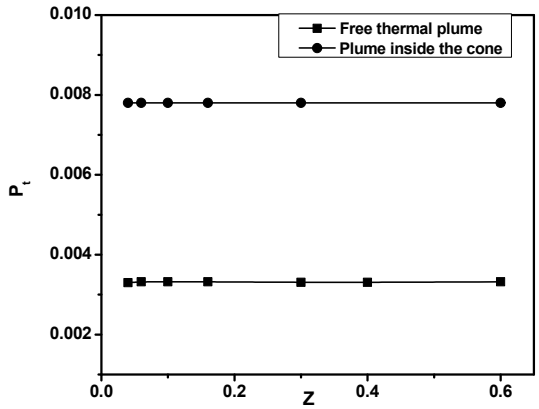


Fig.32. Comparison of the development of the flux absorbed by the air of the free plume and the plume inside the cone.

4.3.3. Air entrainment coefficient

Table 2 presents a comparison of the two configurations' air entrainment coefficient with previous studies. This table shows that the walls surrounding the plume significantly improved the air entrainment coefficient. Compared with prior studies, the confined plume'sair entrainment coefficient was comparable to heated jets. The relative increase in the plume's air entrainment coefficient under the cone walls' effects was 28%. This increase was comparable to the increase in the confined plume's mass flow rate.

4.3.4. Dynamic turbulent intensity

Fig.33 shows a comparison of the turbulence's dynamic axial intensity in the two configurations. In the confined plume, the turbulence intensity was slightly higher above the heat source and decreased more intensely in the flow's second zone. The decrease in the turbulence intensity in the central zone was explained by the strong flow acceleration under the plume contraction's effects. In the flow's last zone, the turbulence intensity was greater in the plume developing inside the cone due to the dominant viscosity forces.

A comparison of the radial distribution of the plume's dynamic turbulent intensity in the two configurations is presented in Figs.34(A-C). As shown in Fig. 34A, in the section near the heat source (Z=0.04), the turbulent intensity was generally higher in the plume evolving inside the cone. Due to the conical walls, the turbulence intensity had a three-extrema profile: a minimum on the plume axis and two maxima mid-radii from the source, where the interaction between the plume and ambient air were maximal due to the lateral and vertical air entrainment mechanisms caused by the plume. At (Z=0.1), the cone walls widened the turbulence intensity's profile, where the maxima moved away and positioned outside the source's limits, indicating the plume's strong interaction with its environment (Fig.34B). In the central flow region (Z=0.3), Fig.34C indicates that the cone walls caused a significant radial widening of the turbulence intensity, which weakened under the previously observed flow acceleration's effects.

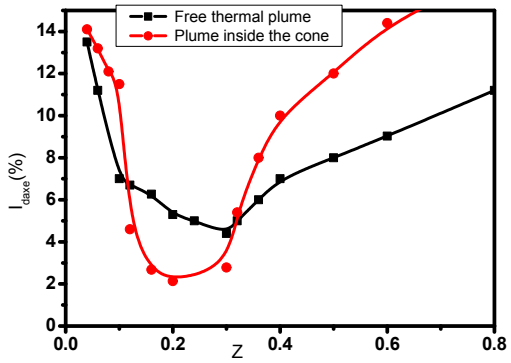


Fig.33. Comparison of dynamic axial intensity of turbulence of the free plume and the plume inside the critical cone.

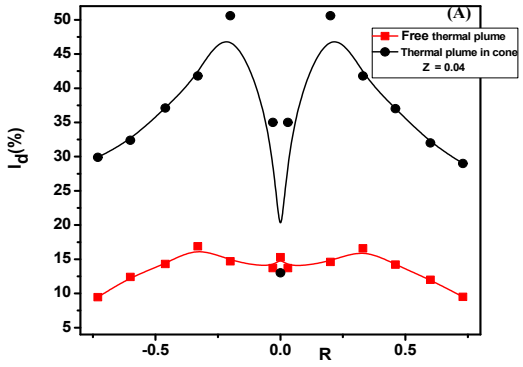


Fig.34. A. Comparison of the distribution of the dynamic turbulent intensity of the free plume and the plume inside the critical cone.

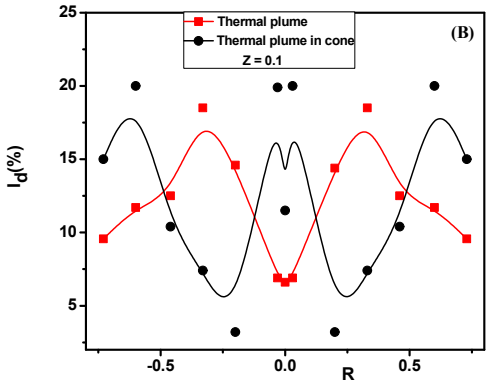


Fig.34. B. Comparison of the distribution of the dynamic turbulent intensity of the free plume and the plume inside the critical cone.

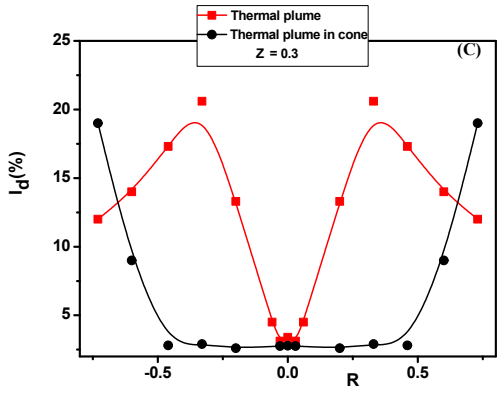


Fig.34. C. Comparison of the distribution of the dynamic turbulent intensity of the plume and the plume inside the critical cone.

4.3.5. Dynamic flatness and skewness factors

Figs.35 and 36 respectively show a comparison of the dynamic flatness and skewness factors' horizontal distribution in the section nearest the heat source (Z=0.04) in the two configurations. Fig. 35 shows the appearance of the maximal values of the dynamic flatness factor at the air inlet's level. Due to the effect of the plume's confinement inside the cone, the maximum moved toward the walls, reflecting the air entrainment supplying the plume. The presence of the negative skewness factor values (Fig. 36) indicated that the plume was no longer supplied with fresh air at its axis level, but through the source's boundaries under the conical walls' effects. The positive skewness factor value demonstrated the heated air's dominance. The zero skewness factors on both sides of the heat source translated into equiprobability in the presence of the heated and fresh air.

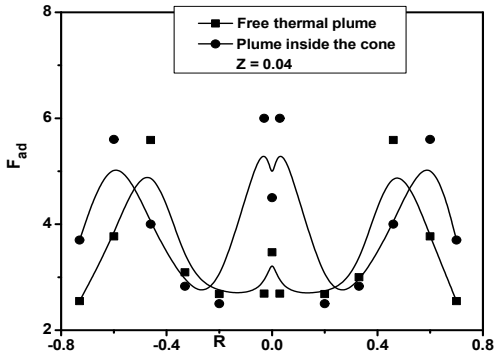


Fig.35. Radial distribution of the dynamic flatness factor of the free plume and the plume inside the critical cone.

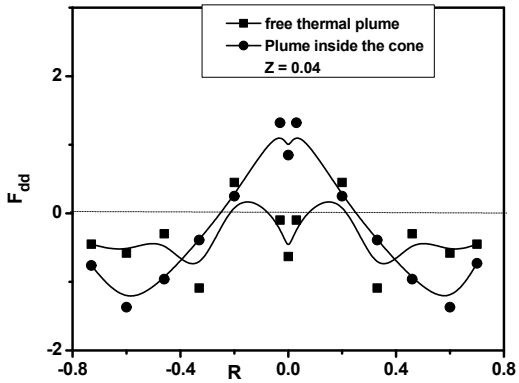


Fig.36. Comparison of the radial distribution of the dynamic skewness factor of the free plume and the plume inside the critical cone.

5. Conclusion

This study experimentally determined the effects of cone walls with a low opening angle

on a thermal plume induced by a heated disc mounted above ground height to ensure regular lateral and vertical air entrainment. The results indicated that the cone walls:

- considerably modified the plume's thermal and dynamic structure;
- significantly widened the plume's radial structure;
- improved the mass flow rate and convective heat flux;
- increased the plume's airentrainment coefficient.

The influence of inclined walls on a plume's flow structure is as important as the cone's opening angles. Studying these walls' effects on a plume's convective transfer and structure is necessary to elucidate the air entrainment mechanisms.

References

[1] H. Stommel, Entrainment of air into a cumulus cloud. J. of Meteorology. 4 (1947) 91-94.

[2] H. G. Houghton, H. E. Cramer, A theory of entrainment in convective currents, J. of Meteorology. 8 (1951) 95 -102.

[3] B. R. Morton, Forced plumes. J. Fluid Mech. 5 (1958) 151-163.

[4] G. I. Taylor, Dynamics of a mass of hot gas rising in air. US Atomic Energy Commission MDDC-919LADC-276 (1945).

[5] H. Mishra, J. Philip, Experimental study ofturbulent jets and forced plumes : Entrainment profiles coefficient and prediction from some existing models. 11th Int. Symposium on turbulence and shear flow phenomena, Southampton, UK, July 30 to August 2, (2019).

[6]V. Reeuwijk, M. Salizzoni, P. Hunt, G. R. Grask, Turbulent transport and entrainment in jets and plumes. Physical Review Fluids, 1 (2016) 1- 22.

[7] H. M. Seyyed, J. Griffin, C. Beckermann, Simulation of air entrainment during mold filling: Comparison with water modeling experiments. Metallurgical and Materials transactions B. 49B (2018) 2599-2610.

[8] B. R. Morton, G. Taylor, J. S. Turner, Turbulent gravitational convection from maintained and instantaneous sources. Proc. Roy. Soc. A 234 (1956) 1–23.

[9] S. L. Lee, H.W. Emmons, A study of natural convection above a fine fire. J. Fluid Mech. 11 (1962) 353 – 368.

[10] E. Kaminski, S. Tait, G. Carrazo, Turbulent entrainment in jets with arbitrary buoyancy. J. Fluid Mech. 526 (2005) 361-376.

[11] E. J. List, J. Imberger, Turbulent entrainment in buoyant jets and plumes. J. Hydr. Div. A.S.C.E. 101 (1975) 617 -620.

[12] N. E. Kotsovinos, E.J. List, Plane turbulent buoyant jets, Part I: Integral Proprieties. J. Fluid Mech. 81, (1977) 25 - 44.

[13] P. M. Tate, The rise and dilution of buoyant jets and their behaviour in an internal wave field, Phd. Thesis, University of New South Wales (2002).

[14] F. P. Ricou, D. B. Spalding, Measurements of entrainment by axisymmetrical turbulent jets. J. Fluid Mech. 11 (1961) 21-23.

[15] M. Brahimi, Structure turbulente des panaches thermiques. Thèse, Université de Poitiers. (1987).

[16] A. Matulka, P. Lopez, J. M. Redondo and A. Tarquis, On the entrainment coefficient in a forced plume: Quantitative effect of source parameters. Nonlinear Processes in Geophysics. 21 (2014) 2 - 10.

[17] Y. Li, R. Hu, L. Yi, G. Wang, Experimental studies on the effects of the fire position on plume entrainment in a large space. Int. J. of Engineering Performance- Based fire codes. 5 (2003) 138-145.

[18] J. M. Agator, Contribution à l'étude de la structure turbulente d'un panache à symétrie axiale. Thèse, Université de Poitiers. (1983).

[19] M. Brahimi, D. K. Son, Experimental investigation and numerical prediction of the mean flow of a turbulent pure plume. Arch. Mech. 38 (1986) 5-6.

[20] Y. Jalura, B. Gebhart, On the buoyancy-induced flow arising from a heated hemisphere, Int. J. Heat and Mass Transfer. 18 (1975) 415 – 431.

[21] H. Nakagome, M. Hirata, The structure of turbulent diffusion in an axisymmetric thermal plume, in:Proc. Int. Sem. Tur. Buoy. Conv., Dubrovnik, Yugoslavia, PP: 361-375, (1976).

[22] W. K. George, R. L. Alpert and F. Tamanini, Turbulence measurement in axisymmetric buoyant plume. J. Heat Mass Transfer. 20 (1977) 1145-1154.

[23] B. Guillou, Etude numérique et expérimentale de la structure turbulente d'un panache à symétrie axiale. Thèse, Université de Poitiers. (1984).

[24] B. Guillou, M. Brahimi, D. K. Son, Structure turbulente d'un panache thermique : Aspect dynamique. J. Méc. Théo. Et Appl. 2 (1986) 371- 401.

[25] H. Q. Yang, Buckling of a thermal plume. Int. J. Heat and Mass Transfer. 35 (1992) 1527 – 1532.

[26] A. Bouzinaoui, R. Devienne, J. R. Fontaine, An experimental study of the thermal plume developed above a finite cylindrical heat source to validate the point source model. Experimental Thermal and Fluid Science. 31 (2007) 649-659.

[27] A. O. M. Mahmoud, J. Bouslimi, R. B. Maad, Experimental study of the effects of a thermal plume entrainment mode on the flow structure: Application to fire. Fire Safety Journal. 44 (2009) 475-486.

[28] J. M. Agator, D. K. Son, Turbulent structure of axisymmetric thermal plumes. Mech. Res. Communication. 9 (3) (1982).

[29] A. O. M. Mahmoud, Etude de l'interaction d'un panache thermique à symétrie axiale avec un écoulement de thermosiphon. Thèse, Université de Tunis II. (1998).

[30] J. Zinoubi, R. Ben Maad, A. Belghith, Influence of the vertical source – cylinder spacing on the interaction of a thermal plume with a thermosiphon flow: an experimental study. Experimental Thermal and Fluid Science 28 (2004) 329-336.

[31] J. Bouslimi, Etude de la structure turbulente d'un panache thermique se développant à l'intérieur d'un cylindre vertical. Thèse, Université de Tunis El Manar, (2005).

[32] J. Bouslimi, L. Dehmani, Experimental investigation of the thermal field for a turbulent plume guided by a cylinder-Preliminary results. Experimental Thermal and Fluid Science, 29 (2005) 477 – 484.

[33] T. Naffouti, J. Zinoubi, R. Ben Maad, Experimental characterization of a free thermal plume and in interaction with its material environment. Applied Thermal Engineering. 30 (2010) 1632-1643.

[34] H. Saafi, A.O.M. Mahmoud, R. B. Maad, Experimental study of the structure of a thermal plume inside a rectangular tunnel. J. of Applied Physics. 4 (2013) 18-25.

[35] P. Kofoed, P. V. Nielsen, Thermal plumes in ventilated rooms, Proc.Roomvent'90, Int. Conf. in Oslo, (1990).

[36] D. Kim Son, M. Stage, J. Coutanceau, Transferts de chaleur entre un fil anémométrique court et un écoulement permanant à faible vitesse. Rev. Gén. Therm. 168 (1975) 951-956.

[37] A. O. M. Mahmoud, Z. yahya, Improvement in the performance of a solar hot air generator using a circular cone. Int. Review of Mechanical Engineering. 13 (2019) 481-492.

[38] B. Guillou, D. K. Son, Etude théorique du développement d'un panache thermique à symétrie axiale : Influence des propriétés thermophysiques du fluide. Int. Comm. Heat Mass Transfer. 10 (1983) 101 -109.

[39] J. Zinoubi, T. Naffouti, L. Thamri, On the experimental analysis of the heating effect of open channel on thermal and dynamic characteristics of resulting flow plume-thermosiphon. American Journal of Engineering Research, 7 (2018) 89 -106.